

Simulating Temperature Transients in First Year Sea Ice

Nitay Ben Shachar¹, Mark McGuinness¹, and Joe Trodahl²

¹Victoria University of Wellington, School of Mathematics and Statistics

²Victoria University of Wellington, School of Chemical and Physical Sciences

November 24, 2022

Abstract

A dynamic one-dimensional model of the freezing of first-year sea ice with a snow cover is presented along with Matlab code. The model is based on historical models in the literature, and is primarily intended to design a computational tool that accurately simulates transient temperature changes within growing sea ice. This may complement temperature data at various depths and times in growing sea ice. The model is validated by comparing the simulated ice temperature profile and growth rate to thermistor temperature profiles measured in 1997 in McMurdo Sound, Antarctica. This comparison shows evidence of platelet ice growth. Despite this, an accuracy of ± 0.4 °C is achieved throughout the entire ice temperature profile, when comparing simulated transient temperatures to data. The model is also used, with the inclusion of a 15mm thick snow layer, to correct a previously observed discrepancy between ice growth rates measured via banding structures in ice cores and the predictions of a steady state ice growth model.

Simulating Temperature Transients in First Year Sea Ice

Nitay Ben Shachar, Mark McGuinness, Joe Trodahl

June 3, 2020

Abstract

A dynamic one-dimensional model of the freezing of first-year sea ice with a snow cover is presented along with Matlab code. The model is based on historical models in the literature, and is primarily intended to design a computational tool that accurately simulates transient temperature changes within growing sea ice. This may complement temperature data at various depths and times in growing sea ice. The model is validated by comparing the simulated ice temperature profile and growth rate to thermistor temperature profiles measured in 1997 in McMurdo Sound, Antarctica. This comparison shows evidence of platelet ice growth. Despite this, an accuracy of $\pm 0.4^\circ\text{C}$ is achieved throughout the entire ice temperature profile, when comparing simulated transient temperatures to data. The model is also used, with the inclusion of a 15mm thick snow layer, to correct a previously observed discrepancy between ice growth rates measured via banding structures in ice cores and the predictions of a steady state ice growth model.

1 Introduction

The modelling of first year sea ice is a vital component of climate modelling, it dictates ocean-atmosphere coupling, and it has implications for long term climate behaviour [17]. First year sea ice forms on open water when air temperatures are below freezing. It grows to a depth of about 1-2m, in contrast to multi year sea ice which stays frozen all year round and is generally thicker.

Simple steady state heat transport models of first year sea ice fail to fully explain measured sea ice growth rates, especially near the surface of the ice [21]. This discrepancy is interpreted as being due to the lack of a modelled snow layer, which if present would impede the ice growth rate, such as in [21]. This, together with an increasing availability of thermistor temperature data recorded versus depth over time as first year ice grows, motivates our development of a rigorous numerical simulator of transient ice temperatures versus depth based on energy conservation. The simulator can be used to study the effects of factors such as snow cover, oceanic heat flux, and salinity profiles, while maintaining accurate calculations of ice thickness versus time.

Sea ice begins to form when the atmosphere cools the surface of the sea sufficiently that many small ice crystals begin to form (frazil ice) [18, 8]. These crystals are agitated by winds and currents so that they are randomly oriented in a mush at the surface of the sea. Once the mush reaches a thickness of approximately 10cm [8, 19] it sets into a solid ice sheet.

After the ice sheet is formed, growth by the addition of frazil crystals becomes negligible, and crystals in the sheet oriented with the direction of most rapid growth close to vertical begin to dominate the ice growth process, forming columnar ice. The extraction of heat via conduction through the ice to the cold atmosphere (relative to the ocean) or to supercooled ocean currents [2, 5] causes columnar ice to further thicken.

At locations like McMurdo Sound, Antarctica, the presence of nearby ice shelves may significantly affect the growth of sea ice. Currents arriving under sea ice from an ice shelf can carry supercooled water within which platelet ice may form. Platelet ice is made up of ice crystals that form in supercooled water. They are buoyant, and may rise and attach to the sea ice from below. As the sea ice sheet continues to thicken due to heat loss to the atmosphere, these crystals may become

incorporated and frozen into the solid ice [22], altering the observed crystal orientation within the sea ice.

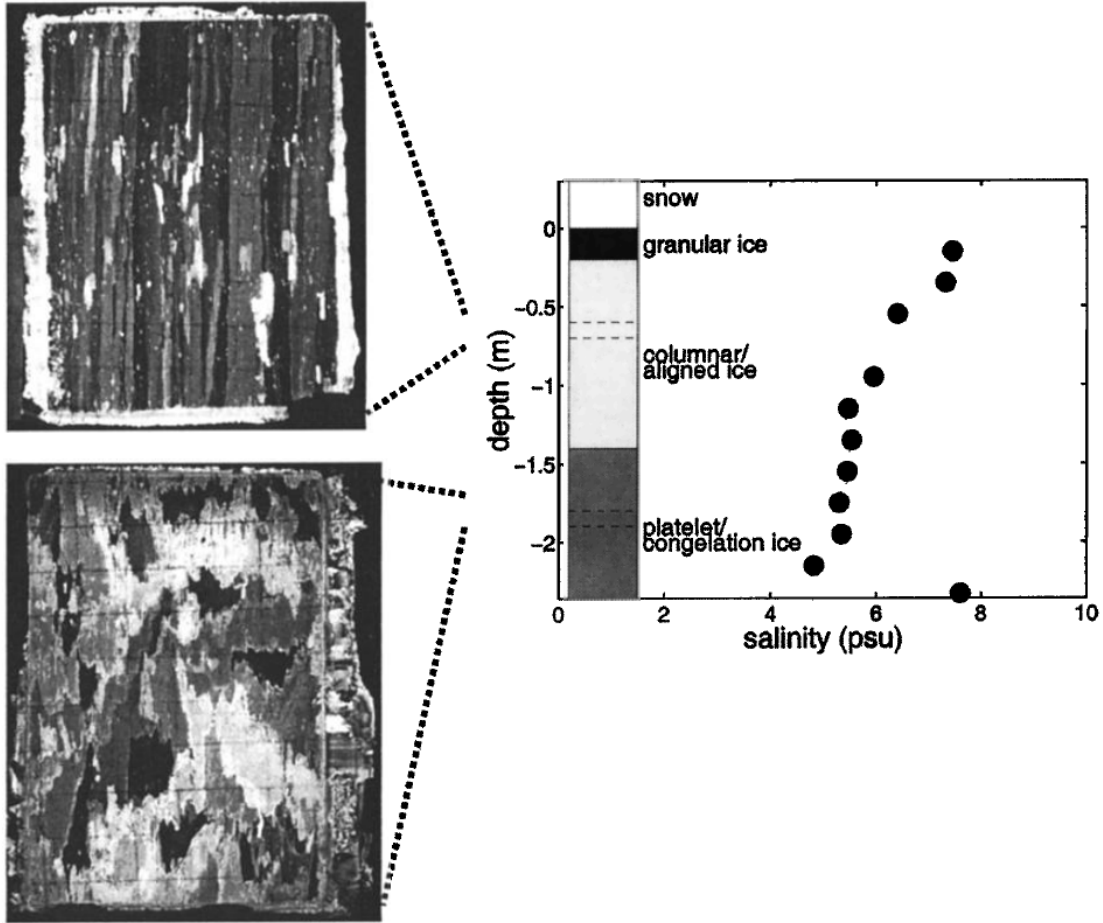


Figure 1: Reprinted from [20]. Ice core data taken near the temperature array in November 1997. The crystal orientations, viewed under crossed polarisers, change from aligned to random, giving insight to the presence or absence of platelet ice.

This mechanism does not depend on heat conduction to a cold atmosphere, and may be incorporated into simulations through the oceanic heat flux term. The presence of platelet ice can be verified by examining the crystal structure of ice cores. Since columnar ice has a preferred growth orientation, it can be distinguished from randomly oriented platelet ice crystals which have been frozen in to the ice, as illustrated in figure 1.

The salinity of sea ice greatly affects its physical properties, which have been studied extensively [25, 12]. Trapped brine travels vertically in pockets, causing a dynamic salinity profile in the ice, and can carry heat when brine drains through tubes in the sea ice [23]. The pockets also travel slowly in the direction of increasing temperature. The bulk thermal properties have been adjusted in accordance with measurements, as detailed in appendix A.

Snow adds an insulating layer between the atmosphere and sea ice, inhibiting heat extraction from the ocean. The snow compresses over time under its own weight and further precipitation, changing its thermal properties. Further, snow thickness is greatly variable due to winds and atmospheric conditions.

An oceanic heat flux term is also usually required in a simulation of heat transport through sea ice. This heat flux is positive (upwards) when the ocean is warmer than the atmosphere. A negative oceanic heat flux can be used to parameterise the growth of sea ice due to accretion of platelet ice

at the ice/ocean interface, when the growth rate is not accounted for by the temperature gradient in the ice at this interface.

In this paper transient heat flow through ice and an overlying snow layer are simulated and solved simultaneously with the changing location of the ice/ocean interface. The Matlab code we use is freely available on GitHub [14]. The user will be able to set the thickness versus time of the snow cover, the time-varying oceanic heat flux, and the salinity.

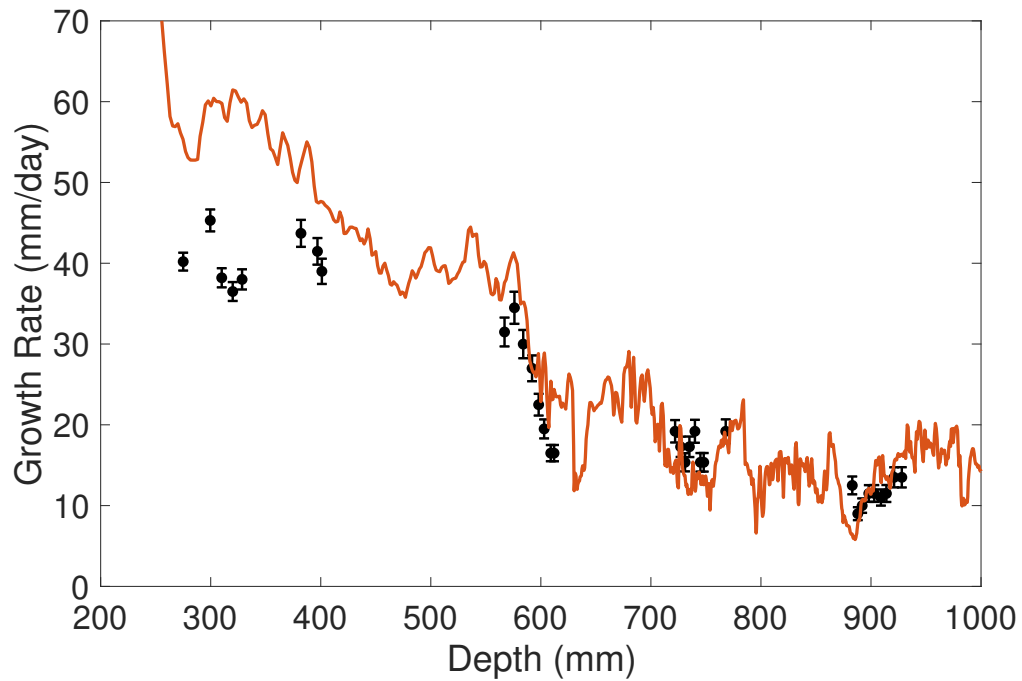


Figure 2: Following [21], ice growth rates from a steady state model using recorded air temperatures (solid line) are compared with growth rate measurements calculated from banding structures observed in ice cores (symbols).

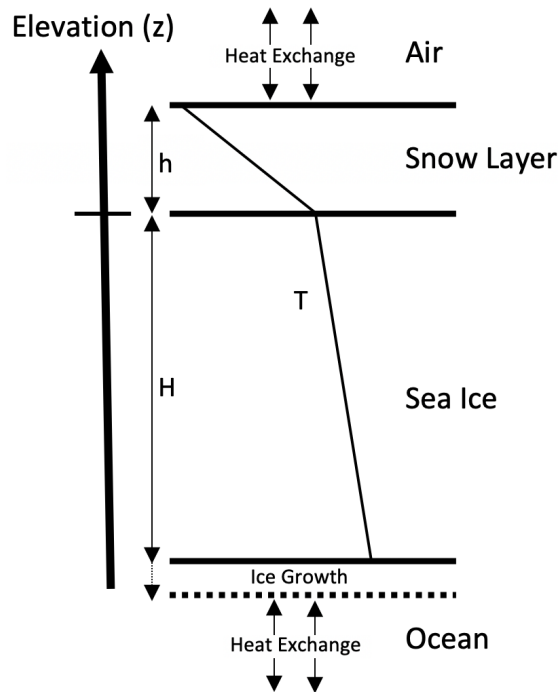


Figure 3: Following [6], this sketch illustrates the fundamental heat exchanges that occur as sea ice grows. An example temperature profile is labeled T with arbitrary units in the horizontal direction.

2 Heat Flow in Sea Ice and Snow

We consider the processes that take place immediately after a solid ice sheet has formed. An existing one-dimensional transient model for the heat flow through growing sea ice is adapted and overlain with a snow layer of variable thickness, with a moving freezing ice/ocean boundary. We develop code [14] to numerically solve for temperature versus elevation and time, to a precision specified by the user, following the work of [7, 6] and inspired by [1, 3, 24]. The model is designed to simulate the growth of first year sea ice due to net heat loss to a cold atmosphere, possibly modified by an oceanic heat flux. The model is not designed to simulate the melting of sea ice, or the formation of slushy layers at the snow/ice interface.

The elevation of the ice/ocean interface is $z = H(t)$. The origin $z = 0$ is set at the ice/snow interface, so that $H < 0$ and ice thickness is $|H|$. The thickness of the snow cover is directly specified by the user, and is given by the non-negative elevation value $z = h(t)$. Inside the ice and the snow we require conservation of energy, so that ignoring solar radiation, the temperature $T(z, t)$ of ice satisfies

$$\rho c \frac{\partial T}{\partial t} = \frac{\partial}{\partial z} \left(k \frac{\partial T}{\partial z} \right), \quad z \in [H, 0], \quad (1)$$

where ρ is ice density, c is thermal capacity, and k is the thermal conductivity of sea ice.

A similar equation holds for the temperature T^s in the snow, if present, for $z \in [0, h]$. The boundary conditions are

- Ocean-ice interface, at the moving boundary $z = H(t)$ the ice must be at the freezing temperature,

$$T(H(t), t) = T_{\text{freezing}}. \quad (2)$$

The ice growth rate is determined by an energy balance — the heat required to be extracted

to freeze liquid to ice is provided by the net heat flux at this interface:

$$k \frac{\partial T}{\partial z} \Big|_H + W_{\text{ocean}} = \frac{dH}{dt} L \rho. \quad (3)$$

The first term on the left hand side is the heat flux to the interface due to the temperature gradient in the sea ice. During ice growth due to a cold atmosphere, this term is usually negative.

The term W_{ocean} is the oceanic heat flux, the flow of heat to the interface from the underlying ocean. It is commonly associated with the following mechanisms:

- Super-cooled water just below the ice-ocean interface
- Platelet ice growth
- Heat flux from a relatively warm ocean current

The right hand side, which is negative if the ice is thickening, is the heat flux required to freeze ice at the rate dH/dt , given the specific latent heat of fusion L .

- If snow is present, the temperature at the top of the snow $z = h(t)$ is set to the current air temperature T_{air} . If there is no snow present, the temperature at the top of the ice $z = 0$ is set to T_{air} . The model is easily modified to a mixed boundary condition relating temperature and gradient, if the user wishes to simulate the effects of a thermal boundary layer in the air flow over the surface.
- If snow is present, at the ice/snow interface $z = 0$ the temperature is required to be continuous

$$T = T^s$$

and the heat fluxes satisfy the energy balance

$$k \frac{\partial T}{\partial z} \Big|_{z=0} = k_s \frac{\partial T^s}{\partial z} \Big|_{z=0} \quad (4)$$

where k_s is the thermal conductivity of snow.

2.1 Discretization and Freezing the Boundary

The boundary between ice and ocean is moving. It is convenient for numerical simulation to make an exact transformation to new spatial coordinates in which this boundary is stationary (*frozen*). The transformation is originally due to Landau [4]. The thickness of the snow cover is also possibly time-varying, and is set by the user. This too can be frozen by a Landau transformation. This simplifies the meshing used to simulate, and avoids the inaccuracies inherent in interpolating if the boundary is moving. We transform using Landau transformations to a new depth variable $\xi = \frac{z}{H(t)}$ for ice and $\chi = \frac{z}{h(t)}$ for snow, so that the snow/air boundary is fixed at $\chi = 1$, the ice/ocean boundary is fixed at $\xi = 1$, and both coordinates have their origin at the ice/snow boundary. For all times, the temperature profiles are now represented on the depth ranges $\xi, \chi \in [0, 1]$.

The chain rules for changing variables are, in the ice

$$\begin{aligned} \frac{\partial}{\partial t} \Big|_z &= \frac{\partial}{\partial t} + \frac{\partial \xi}{\partial t} \frac{\partial}{\partial \xi} = \frac{\partial}{\partial t} - \xi \frac{\dot{H}(t)}{H(t)} \frac{\partial}{\partial \xi} \\ \frac{\partial}{\partial z} &= \frac{\partial \xi}{\partial z} \frac{\partial}{\partial \xi} = \frac{1}{H(t)} \frac{\partial}{\partial \xi} \end{aligned}$$

and similarly in the snow,

$$\begin{aligned} \frac{\partial}{\partial t} \Big|_z &= \frac{\partial}{\partial t} - \chi \frac{\dot{h}(t)}{h(t)} \frac{\partial}{\partial \chi} \\ \frac{\partial}{\partial z} &= \frac{1}{h(t)} \frac{\partial}{\partial \chi} \end{aligned}$$

Transforming the heat equation for the ice temperature to the scaled depth variables gives

$$\frac{\partial T}{\partial t} = \frac{1}{\rho c H^2} \frac{\partial}{\partial \xi} \left(k \frac{\partial T}{\partial \xi} \right) + \xi \frac{\dot{H}}{H} \frac{\partial T}{\partial \xi}, \quad \xi \in [0, 1]. \quad (5)$$

Similarly for snow,

$$\frac{\partial T^s}{\partial t} = \frac{1}{\rho^s c^s h^2} \frac{\partial}{\partial \chi} \left(k^s \frac{\partial T^s}{\partial \chi} \right) + \chi \frac{\dot{h}}{h} \frac{\partial T^s}{\partial \chi}, \quad \chi \in [0, 1]. \quad (6)$$

We use the method of lines to solve these coupled partial differential equations, turning them into many coupled ordinary differential equations, to be solved simultaneously with an ordinary differential equation determining H , obtained by rearranging equation (3) as

$$\frac{dH}{dt} = \left(\frac{k}{L\rho} \right) \frac{\partial T}{\partial z} \Big|_H + \frac{W_{\text{ocean}}}{L\rho}. \quad (7)$$

The spatial ice coordinates are discretised with a mesh of constant spacing $\Delta\xi = \xi_i - \xi_{i-1}$, where

$$\xi = \xi_0, \xi_1, \dots, \xi_n, \quad \xi_0 = 0, \xi_n = 1.$$

and we label the time-varying ice temperatures, and the possibly spatially dependent ice properties at these points

$$T_i = T(\xi_i, t), \quad \rho_i = \rho(\xi_i), \quad c_i = c(\xi_i), \quad k_i = k(\xi_i), \quad i = 0, 1, \dots, n$$

The spatial derivatives are approximated using central differences, allowing the thermal conductivity to possibly vary spatially. The flux term is kept second-order accurate, by using

$$\frac{\partial}{\partial \xi} \left(k \frac{\partial T}{\partial \xi} \right) \approx \frac{k_{i+1/2} \left(\frac{T_{i+1} - T_i}{\Delta\xi} \right) - k_{i-1/2} \left(\frac{T_i - T_{i-1}}{\Delta\xi} \right)}{\Delta\xi},$$

where

$$\begin{aligned} k_{i+1/2} &= \frac{k_{i+1} + k_i}{2}, \\ k_{i-1/2} &= \frac{k_i + k_{i-1}}{2}, \end{aligned}$$

to obtain the coupled ordinary differential equations

$$\begin{aligned} \frac{dT_i}{dt} &= \frac{1}{\rho_i c_i H^2} \frac{(k_{i+1} + k_i) (T_{i+1} - T_i) + (k_{i-1} + k_i) (T_{i-1} - T_i)}{2(\Delta\xi)^2} \\ &+ \xi \frac{\dot{H}}{H} \left(\frac{T_{i+1} - T_{i-1}}{2\Delta\xi} \right), \quad i = 1 \dots n - 1. \end{aligned} \quad (8)$$

Similarly, the temperatures T_j^s in the snow region must satisfy

$$\begin{aligned} \frac{dT_j^s}{dt} &= \frac{1}{\rho_j^s c_j^s h^2} \frac{(k_{j+1}^s + k_j^s) (T_{j+1}^s - T_j^s) + (k_{j-1}^s + k_j^s) (T_{j-1}^s - T_j^s)}{2(\Delta\chi)^2} \\ &+ \chi \frac{\dot{h}}{h} \left(\frac{T_{j+1}^s - T_{j-1}^s}{2\Delta\chi} \right), \quad j = 1 \dots m - 1. \end{aligned} \quad (9)$$

These equations, together with the discretised version of equation 7,

$$\frac{dH}{dt} = \left(\frac{k_{n-1/2}}{L\rho_{n-1/2}} \right) \left(\frac{T_n - T_{n-1}}{H\Delta\xi} \right) - \frac{W_{\text{ocean}}}{L\rho_{n-1/2}}, \quad (10)$$

are to be solved simultaneously for the unknown temperatures $T_i(t)$ and $T_j^s(t)$, $i = 1 \dots n - 1$, $j = 1 \dots m - 1$, and for the unknown $H(t)$. The subscripts on ρ are to be interpreted as above for those on k .

The user provides $h(t)$. If no snow layer is desired, h may be set to a relatively small number so that the snow layer has negligible effect.

Solving requires that the boundary values T_0 , T_n , T_0^s , and T_m^s are known. These are provided by the boundary conditions:

- At the ice/ocean interface, $T_n = T_{\text{freezing}}$.
- The ice/snow interface boundary condition at origin is given by $T_0 = T_0^s$, and

$$k_0 \left(\frac{T_1 - T_0}{H \Delta \xi} \right) = k_0^s \left(\frac{T_1^s - T_0^s}{h \Delta \chi} \right).$$

Solving for T_0 gives:

$$T_0 = \frac{H k_0^s T_1^s \Delta \xi - h k_0 T_1 \Delta \chi}{H k_0^s \Delta \xi - h k_0 \Delta \chi}. \quad (11)$$

- At the upper boundary with the atmosphere, the temperature is set to the air temperature if it is available. If there is snow present then

$$T_m^s = T_{\text{air}}, \quad (12)$$

otherwise the temperature of the upper boundary of the ice is set by

$$T_0 = T_{\text{air}}. \quad (13)$$

2.2 Numerical Simulation

Equations 8, 9, and 10 are solved simultaneously together with the boundary conditions, using Matlab's stiff ordinary differential equation solver `ode15s`. More details on the numerical simulation may be found in the code with documentation on GitHub [14].

2.3 Model Limitations

Some limitations of the model include:

- Salt transport is not explicitly modelled, and a fixed salinity profile provided by the user is used (usually this would be estimated from ice core data). The presence of salt affects the thermal properties of the sea ice as detailed in appendix A.
- Snow density and hence its thermal properties vary with age, wind, temperature, and precipitation [25]. For example, snow compresses over time, changing its insulating properties. This is not taken into consideration due to its high variability, and an average value for snow density is used (appendix A).
- Solar radiation is not taken into account, although it can be added relatively easily. During winter growth net heat transport by solar radiation is relatively small. For extensions of the model to include the melt stage in summer, this should be accounted for, as a distributed source/sink term in the differential equations for temperatures.

3 Comparison to Field Measurements

We compare simulated temperatures to field measurements undertaken in McMurdo Sounds, Antarctica, during 1997 [20, 10]. Temperature profiles of the sea ice were obtained by placing thermistors on a 2m rod at intervals of 10cm and freezing it into relatively fresh 90cm thick sea ice in early June. Thermistor temperatures were recorded every half-hour to a data-logger until removal early

in December. Further details such as the instrumentation and location can be found in [20]. We consider temperature measurements starting at the second thermistor to be at spatial origin, the top of the ice, since the first thermistor is inside snow of unknown and varying depth. We use the second thermistor to provide measured values for the upper boundary condition $T = T_{\text{air}}$.

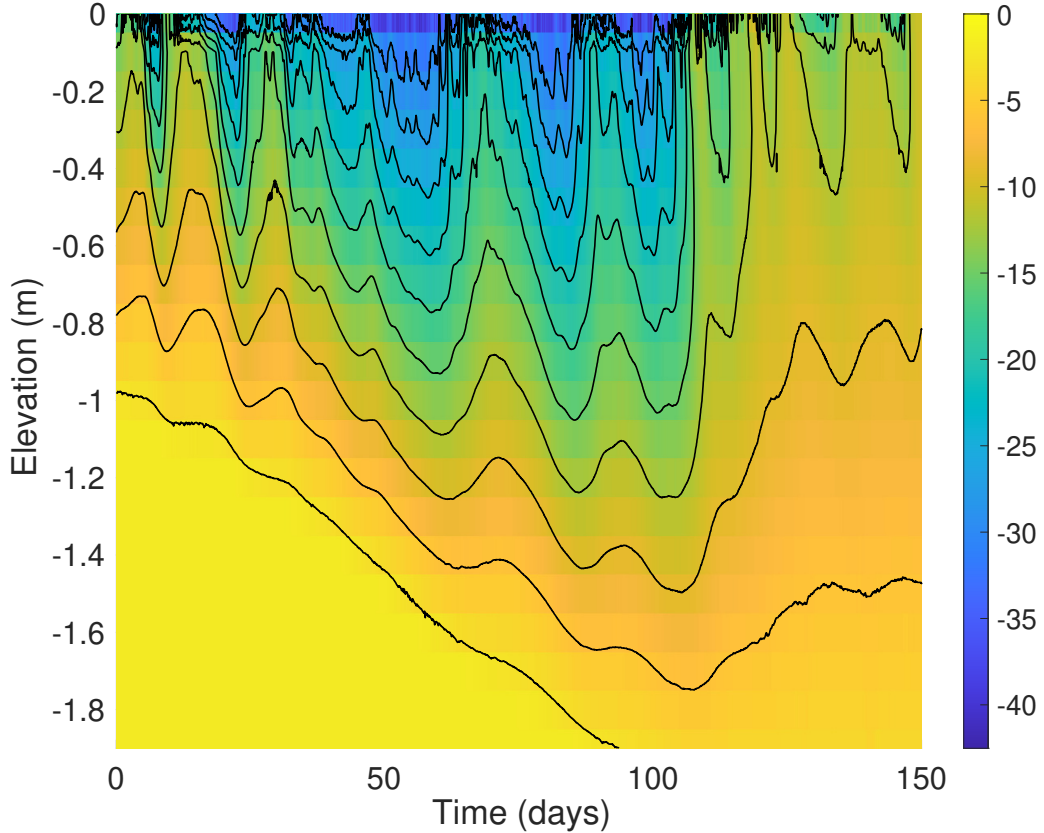


Figure 4: *Temperature array measurements from thermistors deployed in June 1997, as presented in [20]. The colour represents the temperature as indicated by the colour-bar on the right, and contour lines of the temperatures are spaced 3°C apart. The coarse appearance is due to the thermistors being spaced by 10cm, meaning that the spatial resolution of the data is limited to 10cm. The ice is observed to grow from a thickness of about 0.9m to about 1.7m in 80 days. Earlier measurements could not be obtained as the ice was too thin to safely walk on. We also see weather patterns echoed in the temperature recorded at 0m depth, exhibiting slightly cyclic behaviour of period 10-20 days.*

3.1 Ice Thickness Estimation

At each time, we use the temperatures measured with the thermistor array as illustrated in figure 4, to estimate ice thickness, as follows. We observe that the approximate ice depth at time zero say, is between the thermistors located at 0.9m and 1.0m. We estimate from the thermistors an ocean temperature of -1.9°C and using this we investigate the thermistors in the ice immediately before the ice-ocean interface. Then we update our local freezing temperature to be the average of the next two thermistors, those in the ocean but closest to the ice interface, in order to allow for local and possibly time-varying salinity variations. We now fit a straight line to the three temperatures in the sea ice closest to the ice-ocean interface, as illustrated in figure 5. This allows us to extrapolate the temperature profile of the ice and obtain a more accurate estimate for the ice depth. We find the depth where the straight line reaches the estimated freezing temperature, and use this as the ice/ocean interface location, to improve upon the low spatial resolution of the thermistor array. Note that this assumes a 'clean boundary' between the ice and the ocean. This

ignores the effects of a possible mushy layer due to the presence of brine which alters the ice growth mechanism [16, 22, 23].

By smoothing the estimates of ice thickness H (we used splines) and then differentiating the splines with respect to time, an estimate for the growth rate \dot{H} is also obtained directly from thermistor data for comparison purposes. Smoothing is necessary as the data is noisy, giving high variability in growth rates otherwise.

3.2 Estimating Oceanic Heat Flux

The main driver for sea ice growth is the cold air temperature above the ice. The other possible driver is the oceanic heat flux, which is relatively poorly known, and can be estimated on the fly from thermistor data as follows.

The data-based temperature gradients are used together with data-based estimates of H and \dot{H} , to derive the elusive oceanic heat flux term, by using the following rearrangement of equation 3:

$$W_{\text{ocean}} = \dot{H}L\rho - \left(\frac{k}{H}\right) \frac{\partial T}{\partial \xi} \Big|_{\xi=1}. \quad (14)$$

In the process of extrapolating the ice temperature profile provided by data to the boundary with the ocean we also obtain a data-based estimate for the ice temperature gradient at this interface. It is possible to use these temperature gradients based on thermistor data near the boundary of the ocean interface to estimate the amount of ice growth due solely to conduction of heat up through the sea ice, as was done in [13]. Equation 3 rearranges to give

$$\dot{H} = \frac{W_{\text{ocean}}}{L\rho} + \left(\frac{k}{HL\rho}\right) \frac{\partial T}{\partial \xi} \Big|_{\xi=1}, \quad (15)$$

highlighting the two contributors to the growth rate \dot{H} , the oceanic heat flux and the last term, due to the temperature gradient in the ice. These two terms are plotted along with the data-based estimates of growth rate, in figure 6.

3.3 Numerical Simulation of Ice Temperatures

The simulator was run, using thermistor measurements at time zero to provide the initial temperature profile for starting the simulation. Since the uppermost thermistor is inside snow, the second-deepest thermistor was used to set the upper boundary condition at the (model) ice/air interface. A snow layer is then not needed and is not modelled in this section, which tests the accuracy of our numerical model for heat transport solely within the sea ice.

The differences between simulated and measured temperatures are plotted in figure 7, with the ice-ocean interfaces overlaid. In the first simulation oceanic heat flux has been set to zero. The simulated ice growth rate is faster than the data indicates at early times, but is slower than the data indicates after 45 days.

The striped colour patterns visible in figure 7 represent travelling waves of small discrepancies in temperature, possibly due to uncertainties in the salinity values affecting the ice's thermal properties, or to the effect of nearby brine tubes temporarily causing the one-dimensional modelling approach to be less accurate.

A significant transition to a negative oceanic heat flux may be seen in figure 6 when the ice is about 1.4 meters thick, approximately at day 50. This coincides with the first appearance of platelet ice in ice cores (figure 1).

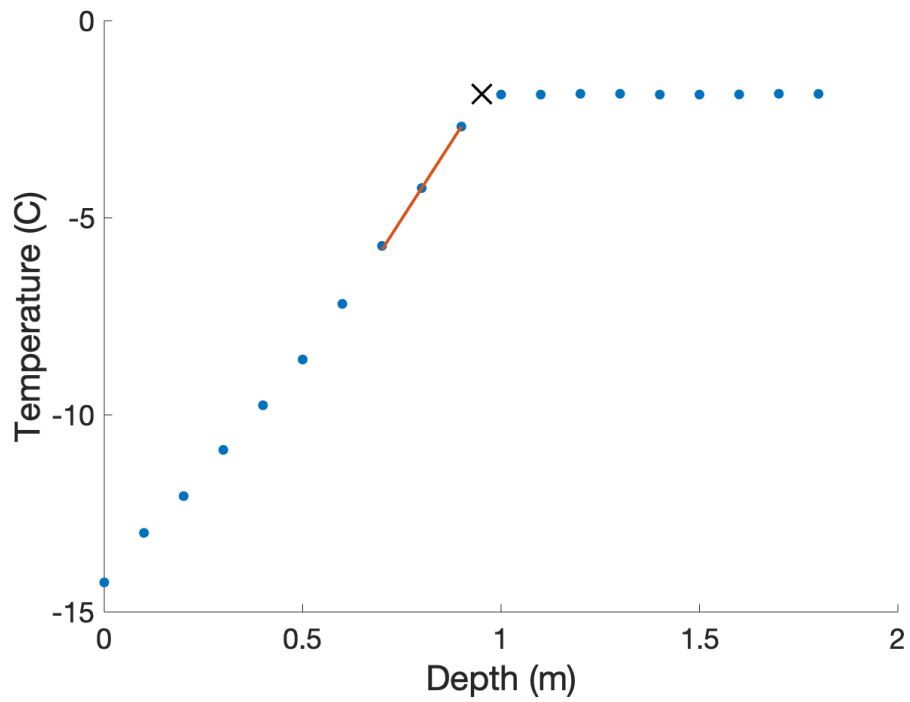


Figure 5: A sketch illustrating how we use the data at each time to infer the location of the ice-ocean interface. A local freezing temperature is calculated directly from the data. The intersection between this and a line fitted to the last three points within the ice gives the estimated interface location (marked by the black x). The gradient of the temperature profile at the interface is estimated as the slope of the fitted red line.

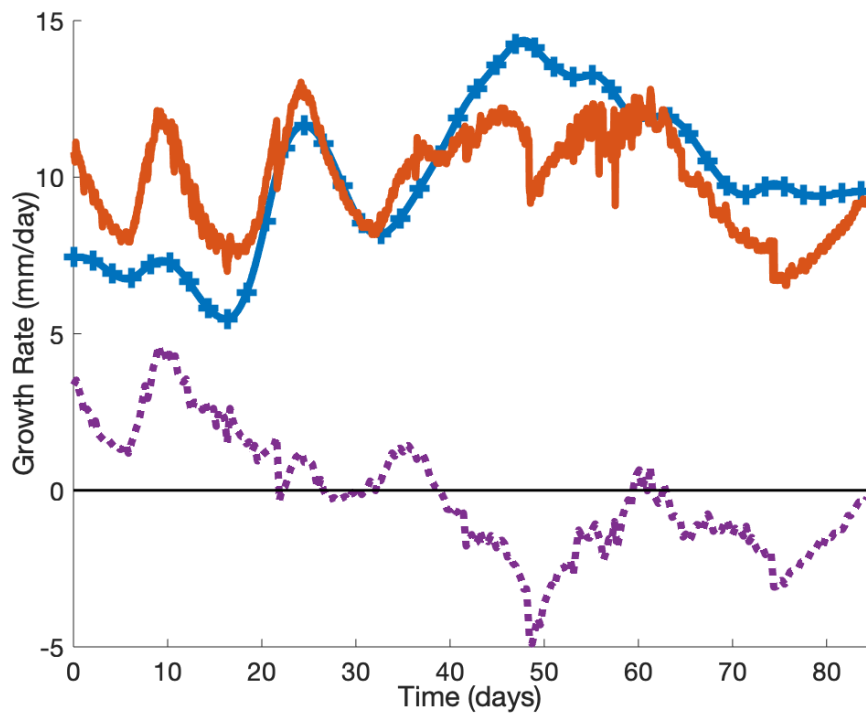


Figure 6: Ice growth rates calculated from temperature data after smoothing (blue solid line with plus symbols) are compared with the temperature gradient contribution to growth rate (solid red line), and with the oceanic heat flux term $\frac{W_{\text{ocean}}}{L\rho}$ (dashed purple line). The temperature gradient term is calculated using the data-based temperature gradient at the ice-ocean interface to compute the last term on the right-hand side of equation 15. The oceanic heat flux W_{ocean} is calculated using equation 14.

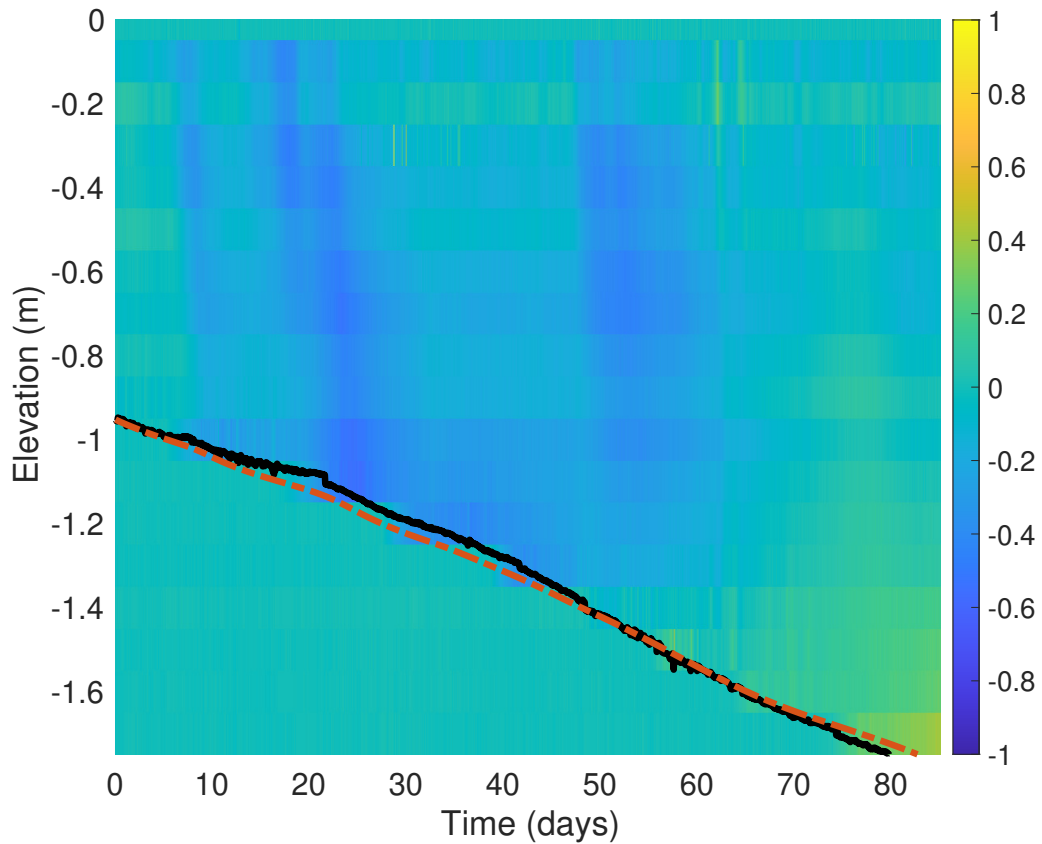


Figure 7: A comparison of measured and simulated temperature profiles and ice thicknesses. Oceanic heat flux is set to zero for the simulations. The colours indicate the temperature difference $T_{\text{data}} - T_{\text{simulated}}$ at each elevation and time. Measured values are taken from the 1997 thermistor array data [20] presented in figure 4. Note that the full colour range for these differences between simulated and measured temperatures is $\pm 1^\circ\text{C}$. The solid black line shows the measured ice/ocean interface elevation estimated from the data, and the dashed red line is the simulated ice/ocean interface elevation.

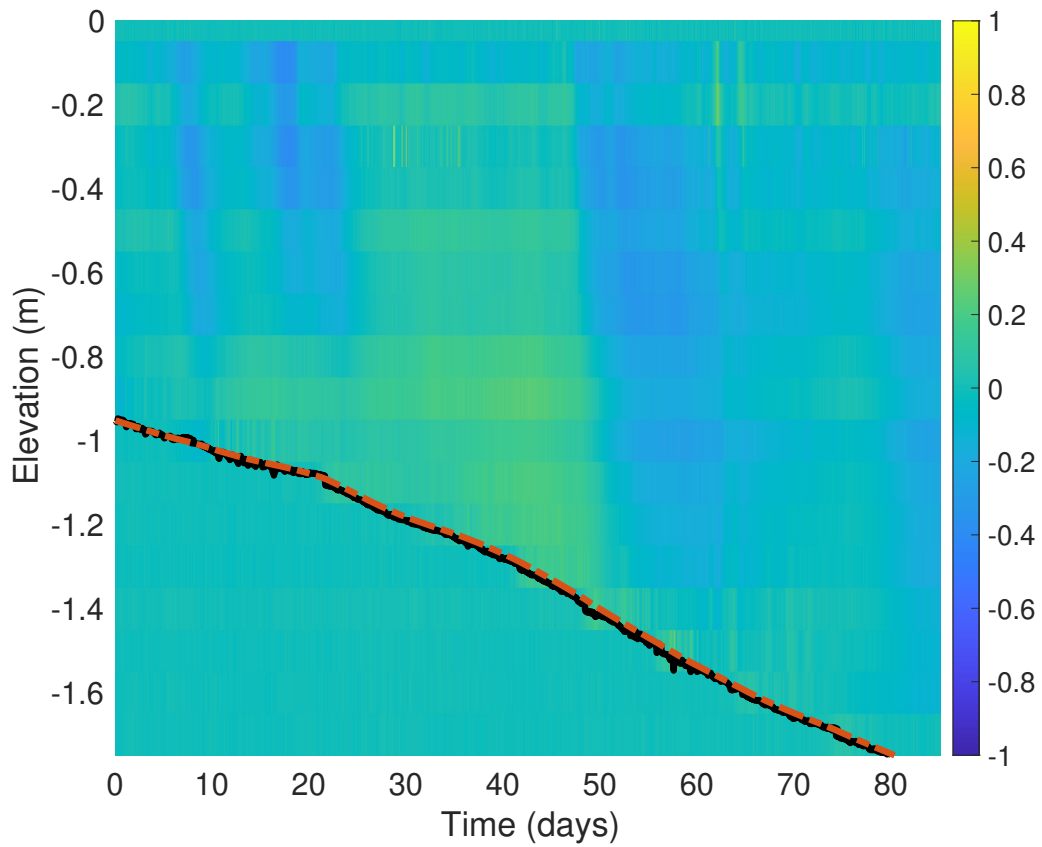


Figure 8: A comparison of measured and simulated temperature profiles and ice thicknesses. The oceanic heat flux used in simulations has been estimated directly from data, as described in section 3.2. Measured temperature values are taken from the 1997 thermistor array data [20] presented in figure 4. The solid black line shows the measured ice/ocean interface elevation estimated using data, and the dashed red line is the simulated ice/ocean interface elevation.

4 Snow Cover

Snow may be added to the model by the user and can vary in thickness with time as desired. Added snow is automatically added at the current air temperature, and snow is removed at the temperatures that currently apply inside the removed snow. Then freshly uncovered snow will be set to the air temperature at the new snow/air interface, but will initially retain its deeper temperature values.

We compare our model simulated results to sea ice growth rates measured via banding analysis performed on an ice core from 1999 in McMurdo Sounds, Antarctica [21]. The banding analysis uses dark bands sometimes seen in young sea ice to infer sea ice growth rate as a function of thickness and can be used to measure growth rates for thin sea ice when a thermistor string cannot safely be deployed. An ice thickness of 110 ± 5 cm was measured using data from a nearby thermistor string [15, 21] on 21 June. Congelation ice formation started at 15cm thickness. The models were tuned to match the sudden rise in air temperatures causing a drop in the growth rates near a thickness of 60cm and to match the final ice thickness. The model presented in [21] was tuned with a freeze in time (15cm thickness of ice) of the early hours of 14 May. Our simulation with no snow had a freeze in time of the early hours of 15 May and with a 15mm snow cover a freeze in time of midday on 11 May. The final thicknesses on 21 June of the simulations were 110cm with no snow and 105cm with 15mm of snow. Both of these are within the measured value range.

With no snow cover the dynamic simulation overestimates the banding-inferred growth rates, and the steady-state model presented in [21] (which also made no allowance for a snow cover) fits the early growth rates more closely than our transient model. This may be due to the different freeze in dates selected to tune each model. When the same freeze in date is selected the transient rates are a closer match to the steady state rates early in the season, but they deviate from the steady state rates later in the season. Furthermore, the latent heat of sea ice used in the steady state model is higher than what we would expect [25] at the typical temperature and salinity of near-freezing sea water, inhibiting the overall modeled growth rates of the steady-state model.

A constant 15mm thick snow cover in the dynamic simulations produces better agreement with banding-inferred growth rates than the no snow models, as may be seen in figure 9. The match is surprisingly good over both early and late times, given the simplicity of the assumption that the snow cover is constant in time. The expected effect of the presence of a snow cover is clearly seen, reducing ice growth rates compared to when there is no snow cover, especially earlier in the season.

The ice core with banding analysis performed to get these measurements was taken about 1km offshore near Arrival Heights in Antarctica in 1999 at a site 150m away from a thermistor string at a latitude/longitude of $77^{\circ}50.197'S$, $166^{\circ}36.764'E$. The thermistor string used has been described in [16] and analysed in [20]. The air temperatures measured at Scott Base [9] were used as a proxy for the air temperatures above the ice for the simulations. Some snow cover was observed to be present at the site when ice cores were taken.

5 Conclusion

A one-dimensional fully transient high resolution thermodynamic model for heat transport in snow and sea ice has been presented as a set of coupled partial differential equations. Moving boundaries have been frozen by using Landau transformations, and the method of lines has been used to replace the partial differential equations with coupled ordinary differential equations describing temperatures in the snow and ice layers, and ice thickness. The Matlab code we used has been made available via GitHub.

The model calculates temperature transients based on the physical parameters of snow and sea ice, coupled with the growth of the sea ice into the ocean in the winter months, driven by cold air temperatures and modified by oceanic heat fluxes.

In a comparison to thermistor string temperature measurements recorded in McMurdo Sound,

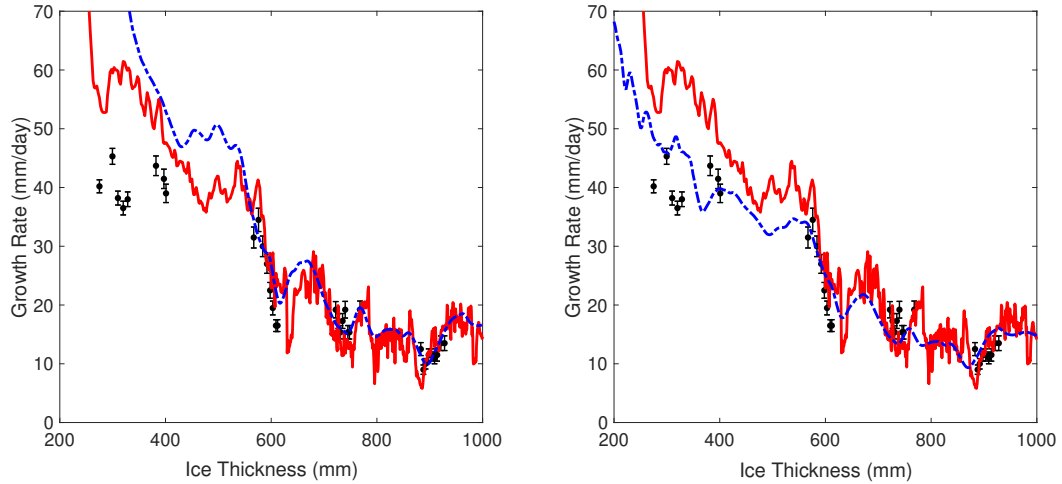


Figure 9: A comparison of ice growth rates computed using a steady state model as in figure 2 and following [21] (solid red curve) with growth rates computed using the new fully transient model presented in this paper (dashed blue curve). Data values are computed from a banding analysis of ice cores (black symbols) [21]. Air temperatures used are those given in [21] **Left:** No snow layer is present in the transient simulations (dashed blue curve). **Right:** A snow layer of constant 15mm thickness has been included in the transient simulations (dashed blue curve).

Antarctica in 1997, the entire data record of measured temperatures is matched by the transient simulations within an accuracy of $\pm 0.4^{\circ}\text{C}$.

A method for calculating oceanic heat flux using thermistor temperature data has been presented. The matches to temperatures and to ice thickness were much improved when oceanic heat flux was included.

Good matches were also obtained to the sea ice thicknesses obtained in a previous publication using the banding observed in sea ice cores from McMurdo Sound in 1999. These matches were obtained by the inclusion of a 15mm layer of snow in the transient simulation.

6 Acknowledgements

Our interest in developing this code was prompted by discussions with Kate E. Turner (Victoria University of Wellington), for which we are grateful.

A Physical Parameters and Constants

All quantities are given in SI units. Temperature is measured in degrees Celsius. Salinity is given in units of grams per gram, note that this is a factor of 1000 smaller than other standard units such as psu, ppt (parts per thousand).

A.1 Ice Properties

- Thermal Conductivity [12] [W/(m K)]:

$$k_{ice} = \frac{\rho}{\rho_i} \left[2.11 - 0.011T + 0.09 \frac{S}{T} - \frac{\rho - \rho_i}{1000} \right]$$

- Heat Capacity [25, 11] [J/(kg K)]:

$$c_{ice} = 1000 \left(2.113 + 0.0075T - 0.0034S \times 1000 + 0.00008ST \times 1000 + 18.04 \frac{S \times 1000}{T^2} \right)$$

- Density [25] [kg/(m³)]:

$$\rho_{ice} = (1 - V_a) \left(1 - \frac{4.51S}{T} \right) 917$$

- Latent Heat of Fusion [25] [J/kg]:

$$L_{ice} = 4184 \left(79.68 - 0.505T - 27.3S + 4311.5 \frac{S}{T} \right)$$

A.2 Snow Properties

- Density [7] [kg/m³]: $\rho_{snow} = 330$
- Thermal Conductivity [25] [W/(m K)]:

$$k_{snow} = 0.0688 \exp \left(0.0088T + 4.6682 \frac{\rho_{snow}}{1000} \right)$$

- Heat Capacity [25] [J/(kg K)]:

$$c_{snow} = (2.7442 + 0.1282(T + 273.15)) \times \frac{18.02}{1000}$$

References

- [1] Bin Cheng et al. “Evolution of snow and ice temperature, thickness and energy balance in Lake Orajärvi, northern Finland”. In: *Tellus A: Dynamic Meteorology and Oceanography* 66.1 (2014), p. 21564. URL: <https://doi.org/10.3402/tellusa.v66.21564>.
- [2] Alexander J. Gough et al. “Signatures of supercooling: McMurdo Sound platelet ice”. In: *Journal of Glaciology* 58.207 (2012), pp. 38–50. DOI: 10.3189/2012JG10J218.
- [3] W. Huang et al. “Modeling experiments on seasonal lake ice mass and energy balance in the Qinghai–Tibet Plateau: a case study”. In: *Hydrology and Earth System Sciences* 23.4 (2019), pp. 2173–2186. URL: <https://www.hydrol-earth-syst-sci.net/23/2173/2019/>.
- [4] H.G. Landau. “Heat conduction in a melting solid”. In: *Quarterly of Applied Mathematics* 8 (1950), pp. 81–94.
- [5] Gregory H. Leonard et al. “Evolution of supercooling under coastal Antarctic sea ice during winter”. In: *Antarctic Science* 23.4 (2011), pp. 399–409. DOI: 10.1017/S0954102011000265.

- [6] Matti Lepparanta. “A review of analytical models of sea-ice growth”. In: *Atmosphere-Ocean* 31.1 (1993), pp. 123–138. URL: <https://doi.org/10.1080/07055900.1993.9649465>.
- [7] Gary A. Maykut and Norbert Untersteiner. “Some results from a time-dependent thermodynamic model of sea ice”. In: *Journal of Geophysical Research (1896-1977)* 76.6 (1971), pp. 1550–1575. DOI: 10.1029/JC076i006p01550. URL: <https://agupubs.onlinelibrary.wiley.com/doi/abs/10.1029/JC076i006p01550>.
- [8] Mark J. McGuinness. “Modelling Sea Ice Growth”. In: *The ANZIAM Journal* 50.3 (2009), pp. 306–319. DOI: 10.1017/S1446181109000029.
- [9] NIWA. *CliFlo*. URL: <https://cliflo.niwa.co.nz/>.
- [10] D. J. Pringle. “Thermal Conductivity of Sea Ice and Antarctic Permafrost”. In: *PhD Thesis, Victoria University of Wellington* (2004).
- [11] D. J. Pringle, H. J. Trodahl, and T. G. Haskell. “Direct measurement of sea ice thermal conductivity: No surface reduction”. In: *Journal of Geophysical Research: Oceans* 111.C5 (2006). DOI: 10.1029/2005JC002990. URL: <https://agupubs.onlinelibrary.wiley.com/doi/abs/10.1029/2005JC002990>.
- [12] D. J. Pringle et al. “Thermal conductivity of landfast Antarctic and Arctic sea ice”. In: *Journal of Geophysical Research: Oceans* 112.C4 (2007). DOI: 10.1029/2006JC003641. eprint: <https://agupubs.onlinelibrary.wiley.com/doi/pdf/10.1029/2006JC003641>. URL: <https://agupubs.onlinelibrary.wiley.com/doi/abs/10.1029/2006JC003641>.
- [13] Craig R. Purdie et al. “Growth of first-year landfast Antarctic sea ice determined from winter temperature measurements”. In: *Annals of Glaciology* 44 (2006), pp. 170–176. DOI: 10.3189/172756406781811853.
- [14] Nitay Ben Shachar. *Sea Ice Growth Modelling*. URL: <https://github.com/nitaybenshahar/Sea-Ice-Growth-Model/>.
- [15] I.J. Smith et al. “Sea ice growth rates near ice shelves”. In: *Cold Regions Science and Technology* 83-84 (2012), pp. 57–70. ISSN: 0165-232X. DOI: <https://doi.org/10.1016/j.coldregions.2012.06.005>. URL: <http://www.sciencedirect.com/science/article/pii/S0165232X12001358>.
- [16] Inga J. Smith et al. “Platelet ice and the land-fast sea ice of McMurdo Sound, Antarctica”. In: *Annals of Glaciology* 33 (2001), pp. 21–27. DOI: 10.3189/172756401781818365.
- [17] T.F. Stocker et al. “Climate Change 2013: The Physical Science Basis. Contribution of Working Group I to the Fifth Assessment Report of the Intergovernmental Panel on Climate Change”. In: *IPCC* (2013). URL: <https://www.ipcc.ch/report/ar5/wg1/>.
- [18] Urban Svensson and Anders Omstedt. “Simulation of supercooling and size distribution in frazil ice dynamics”. In: *Cold Regions Science and Technology* 22.3 (1994), pp. 221–233. ISSN: 0165-232X. DOI: [https://doi.org/10.1016/0165-232X\(94\)90001-9](https://doi.org/10.1016/0165-232X(94)90001-9).
- [19] David Thomas and Gerhard Dieckmann. *Sea Ice: An Introduction To Its Physics, Chemistry, Biology and Geology*. Jan. 2003. ISBN: 0632058080. DOI: 10.1002/9780470757161.ch9.
- [20] H. J. Trodahl et al. “Heat transport in McMurdo Sound first-year fast ice”. In: *Journal of Geophysical Research: Oceans* 105.C5 (2000), pp. 11347–11358. URL: <https://agupubs.onlinelibrary.wiley.com/doi/abs/10.1029/1999JC000003>.
- [21] Kate E. Turner et al. “Sea ice growth rates from tide-driven visible banding”. In: *Journal of Geophysical Research: Oceans* 122.6 (2017), pp. 4675–4684. URL: <https://agupubs.onlinelibrary.wiley.com/doi/abs/10.1002/2016JC012524>.
- [22] Pat Wongpan et al. “Simulation of the crystal growth of platelet sea ice with diffusive heat and mass transfer”. In: *Annals of Glaciology* 56.69 (2015), pp. 127–136. DOI: 10.3189/2015AoG69A777.
- [23] M. Worster and J. Wettlaufer. “Natural convection, solute trapping and channel formation during solidification of salt water”. In: *Journal of Physical Chemistry* B101 (1997), pp. 6132–6136.

- [24] Yu Yang et al. “Numerical modelling of snow and ice thicknesses in Lake Vanajavesi, Finland”. In: *Tellus A: Dynamic Meteorology and Oceanography* 64.1 (2012), p. 17202. DOI: 10.3402/tellusa.v64i0.17202. URL: <https://doi.org/10.3402/tellusa.v64i0.17202>.
- [25] Yin-Chao Yen. “Review of Thermal Properties of Snow, Ice and Sea Ice”. In: (June 1981). URL: <https://apps.dtic.mil/dtic/tr/fulltext/u2/a103734.pdf>.